frontiers in Materials

ORIGINAL RESEARCH
published: 26 November 2020
doi: 10.3389/fmats.2020.578518

Non-precious Melamine/Chitosan Composites for the Oxygen Reduction Reaction: Effect of the Transition Metal

B. Aghabarari[1], M. V. Martínez-Huerta[2], M. C. Capel-Sánchez[2] and M. J. Lázaro[3]**

[1] Department of Nanotechnology and Advanced Material, Materials and Energy Research Center (MERC), Tehran, Iran, [2] Instituto de Catálisis y Petroleoquímica, CSIC, Madrid, Spain, [3] Instituto de Carboquímica, CSIC, Zaragoza, Spain

The development of active and low-cost electrocatalysts for the oxygen reduction reaction (ORR) is crucial for the sustainable commercialization of fuel cell technologies. In this study, we have synthetized Me/Mo_2C (Me = Fe, Co, Cu)-based composites embedded in N- and P-dual doped carbon by means of inexpensive industrial materials, such as melamine and chitosan, as C and N sources, and the heteropolyacid $H_3PMo_{12}O_{40}$ as P and Mo precursor. The effect of the transition metal (Fe, Co, and Cu) on the ORR in alkaline medium has been investigated. The physicochemical properties of the electrocatalysts were performed by X-ray diffraction (XRD), X-ray photoelectron spectroscopy (XPS), Raman spectroscopy, and transmission electron microscopy (TEM). Activity towards ORR was carried out in a three-electrode cell using a ring-disk electrode in 0.1M NaOH. The results obtained clearly show the important role played by each transition metal (Fe, Co, and Cu) in the electrochemical activity. Among them, Fe gives rise to the best performing composite in carrying out the oxygen reduction reaction. The formation Fe_3C/Mo_2C species embedded in N- and P-dual doped carbon seems to be the determining role in the increase of the ORR performance.

Keywords: oxygen reduction, composites, chitosan, melamine, electrocatalyst, heteropolyacid

OPEN ACCESS

Edited by:
Emilia Morallon,
University of Alicante, Spain

Reviewed by:
Jialiang Wang,
University of Wisconsin-Madison, United States
Dongsheng Geng,
University of Science and Technology Beijing, China

****Correspondence:***
M. V. Martínez-Huerta
mmartinez@icp.csic.es
M. J. Lázaro
mlazaro@icb.csic.es

Specialty section:
This article was submitted to Energy Materials, a section of the journal Frontiers in Materials

Received: *30 June 2020*
Accepted: *05 October 2020*
Published: *26 November 2020*

Citation:
Aghabarari B, Martínez-Huerta MV, Capel-Sánchez MC and Lázaro MJ (2020) Non-precious Melamine/Chitosan Composites for the Oxygen Reduction Reaction: Effect of the Transition Metal. Front. Mater. 7:578518. doi: 10.3389/fmats.2020.578518

INTRODUCTION

The oxygen reduction reaction (ORR) is the main electrochemical reaction occurring at the cathode of polymer electrolyte fuel cells. Due to the inherently slow reaction kinetics of the ORR, platinum precious metal is required as an electrocatalyst because of its high activity and durability (Stephens et al., 2012; Shao et al., 2016; Martínez-Huerta and Lázaro, 2017). However, Pt must be substituted or dramatically reduced in the ORR cathode in order to reduce the cost and to ensure sustainable development for commercial applications. The development of active and precious-metal-free catalysts thereby becomes an imperative issue in the field of electrocatalysis (Jaouen et al., 2011; Wang et al., 2019).

One of the most significant ways to reduce the cost and improve the kinetics of the ORR is the utilization of an alkaline environment. In this condition, oxygen is reduced to water at the cathode via two possible reaction pathways: the direct four-electron ($4e^-$) pathway and the energetically undesirable two-stage ($2e^-$) pathway with a peroxide intermediate (Martínez-Huerta and Lázaro, 2017). The elementary reaction routes in alkaline media are (**Eqs 1**, **2**, and **3**):

Direct four-electron pathway: $O_2 + 2H_2O + 4e^- \rightarrow 4OH^-$ (1)

Two-stage pathway: $O_2 + 2H_2O + 2e^- \rightarrow HO_{2^-} + OH^-$ (2)

$HO_{2^-} + OH^- + 2e^- \rightarrow 3OH^-$ (3)

Among non-precious metal catalysts, N-doped carbon with transition metals (for example, Fe or Co) have proven to have remarkably enhanced electrocatalytic activity for ORR in an alkaline environment (Wu et al., 2011; Palaniselvam et al., 2016; Shao et al., 2016; Wang et al., 2019; Yasuda et al., 2016; Wang et al., 2019). Conventionally, these catalysts are synthetized by pyrolysis of mixtures containing a carbon material, a metal salt, and a nitrogen-rich organic compound in the presence of an inert gas. Additionally, N species can be incorporated into the carbon nanostructures by pyrolysis of abundant eco-friendly raw material sources, which has benefits such as low cost or easy synthetic conditions (Chung et al., 2013; Li et al., 2014a; Das and Yurtcan, 2016; Pan et al., 2016; Qiao et al., 2016).

In this study, N-doped carbon matrix is obtained from two low-cost industrial materials, chitosan and melamine. Chitosan is a plentiful, harmless and low cost biopolymer, which is a waste product derivative of the crabbing and shrimp canning industry (Marguerite, 2006). Chitosan has been chosen as both carbon and N sources due to its abundant N-bearing groups (Wu et al., 2015; Xie et al., 2015; Aghabarari et al., 2017; Aghabarari et al. 2013). Qiao et al. prepared graphene/nitrogen-doped porous carbon sandwiches for the metal-free oxygen reduction reaction using chitosan as a nitrogen source (Qiao et al., 2016). Nitrogen doping increased the electrical conductivity and the number and the nature of the active sites for the ORR. Melamine is also a nitrogen-rich organic molecule and low-cost raw material in the chemical industry. Melamine possesses a three-dimensional monoclinic structure which is similar to C_3N_4. Its decomposition favors the incorporation of nitrogen in carbonaceous materials obtained by pyrolysis (Sheng et al., 2011; Liu et al., 2013; Li et al., 2014b; Peng et al., 2014). Rybarczyk et al. also studied the formation of nitrogen-doped porous carbonaceous materials by thermal decomposition of a mixture of chitosan and melamine in an inert atmosphere (Rybarczyk et al., 2015; Khan et al., 2020). They found that, in addition to the entire nitrogen content and the kind of nitrogen group (pyridinic N or quaternary N), the content of carbon "kinks" and/or surface roughness also deeply influenced the ORR activity.

Transition metal carbides are highly attractive since they exhibit electronic and catalytic properties similar to Pt (Guil-López et al., 2010; Roca-Ayats et al., 2014; Zhong et al., 2015). Recently, a number of research groups have demonstrated that molybdenum carbides can be active electrocatalysts for the oxygen reduction reaction (Liao et al., 2014; Fan et al., 2017; Zhang et al., 2017; Li et al., 2019). The physicochemical properties of molybdenum carbides, such as mechanical hardness, thermal stability, singular metal–carbon chemical bonds, and noble-metal-like d-state density around the Fermi level, make them very promising materials for obtaining advanced ORR composites.

Herein, we have synthetized Me/Mo_2C (Me = Fe, Co, Cu)-based composites embedded in N- and P-dual doped carbon using a facile synthesis strategy developed by our research group (Aghabarari et al., 2019). For this preparation, the corresponding metallic precursor and molybdophosphoric acid (HMoP) are pyrolyzed together with the mixture chitosan/melamine as carbon and nitrogen sources. HMoP was used as a source of P and Mo. The effect of the transition metal (Fe, Co, and Cu) on the structure and ORR activity has been investigated. The physicochemical properties of the electrocatalysts were performed by Raman spectroscopy, X-ray diffraction (XRD), X-ray photoelectron spectroscopy (XPS), and transmission electron microscopy (TEM). Activity towards ORR was carried out in a three-electrode electrochemical cell using a ring-disk electrode in 0.1M NaOH.

EXPERIMENTAL

Composites Synthesis

The preparation of the composites follows the synthetic strategy developed by our research group (Aghabarari et al., 2019) and is schematically illustrated in **Figure 1**. For the synthesis of composites, an appropriate amount of the chloride salt precursor (Sigma-Alderich Company) of Co, Fe, or Cu (20 wt % with respect to the composite melamine/chitosan) was dissolved in water and then was added to a solution of chitosan in acetic acid solution. After that, a solution of melamine was added drop by drop to the mixture and stirred vigorously (weight ratio melamine/chitosan = 1/1). In the next step, the appropriate amount of the $H_3PMo_{12}O_{40}$ solution (10 wt % with respect to the composite melamine/chitosan) was added to the mixture and, after 2 h stirring, the solution was dried at 70°C in a vacuum oven. The sample was pyrolized in a tubular quartz furnace at 800°C over 3h. The product was washed with 10 wt% HCl solution. The acid-treated solid sample was filtered and washed with water until free of chlorine ions. Finally, the sample was dried at 70°C in a vacuum oven to obtain the final catalysts. The three catalysts were labeled as Fe/Mo_2C/NPC, Co/Mo_2C/NPC, and Cu/Mo_2C/NPC. For comparison, melamine/chitosan (NPC) composite was also prepared using a similar route but without adding any metal and heteropolyacid into the composite.

Characterization of the Electrocatalytic Materials

X-ray diffraction analyses of the composites were carried out on a PANalytical X'Pert Pro X-ray diffractometer with a Cu Kα source. X-ray Photoelectron Spectroscopy (XPS) data was analyzed with a PHOIBOS 150 9MCD spectrometer with Multi-Channeltron detector fitted with a Mg Kα radiation ($h\nu$ = 1,253.6 eV) and an XRC-1000 X-ray gun. TEM images were obtained using a high resolution of transmission electron microscopy (HRTEM) JEOL 2100F operating at an accelerating voltage of 200 kV. Raman spectroscopy was carried out with a Renishaw in Via Raman

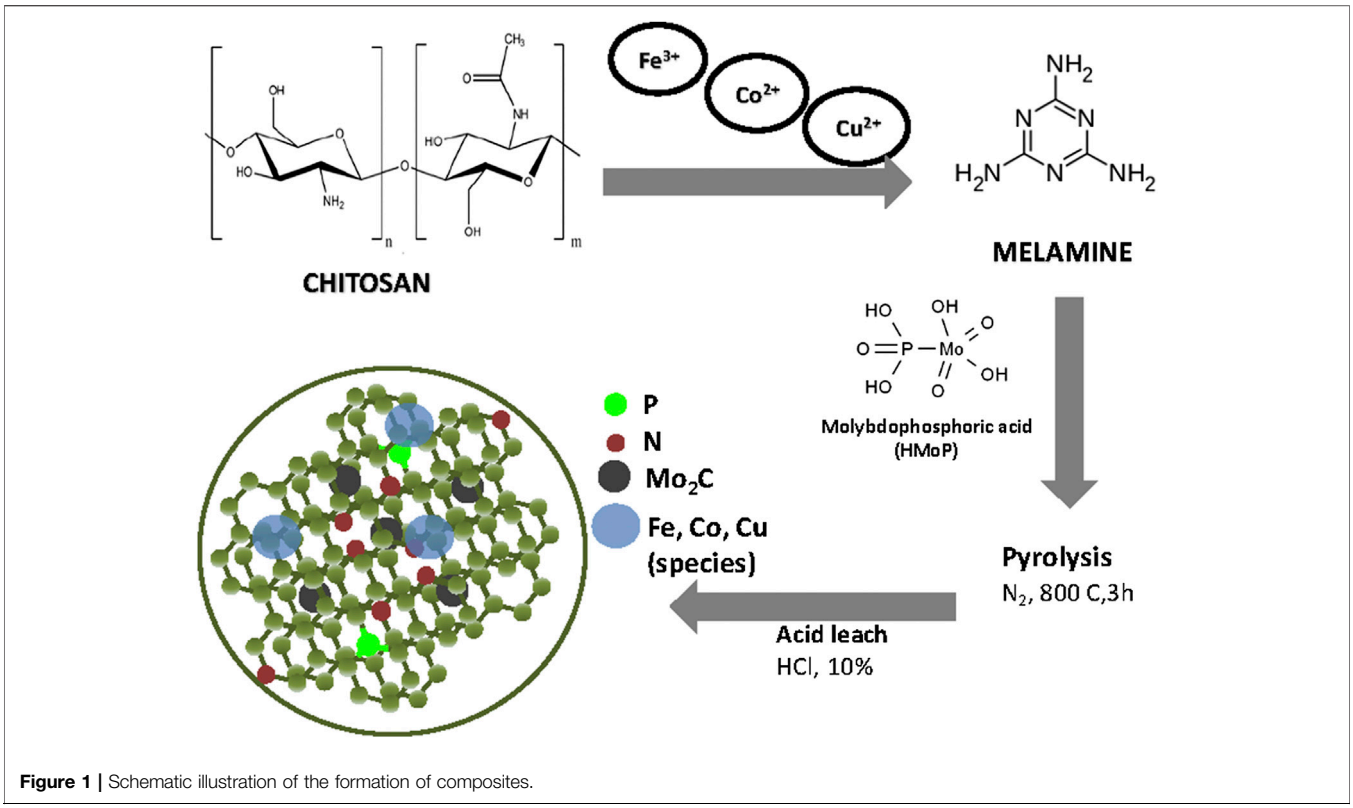

Figure 1 | Schematic illustration of the formation of composites.

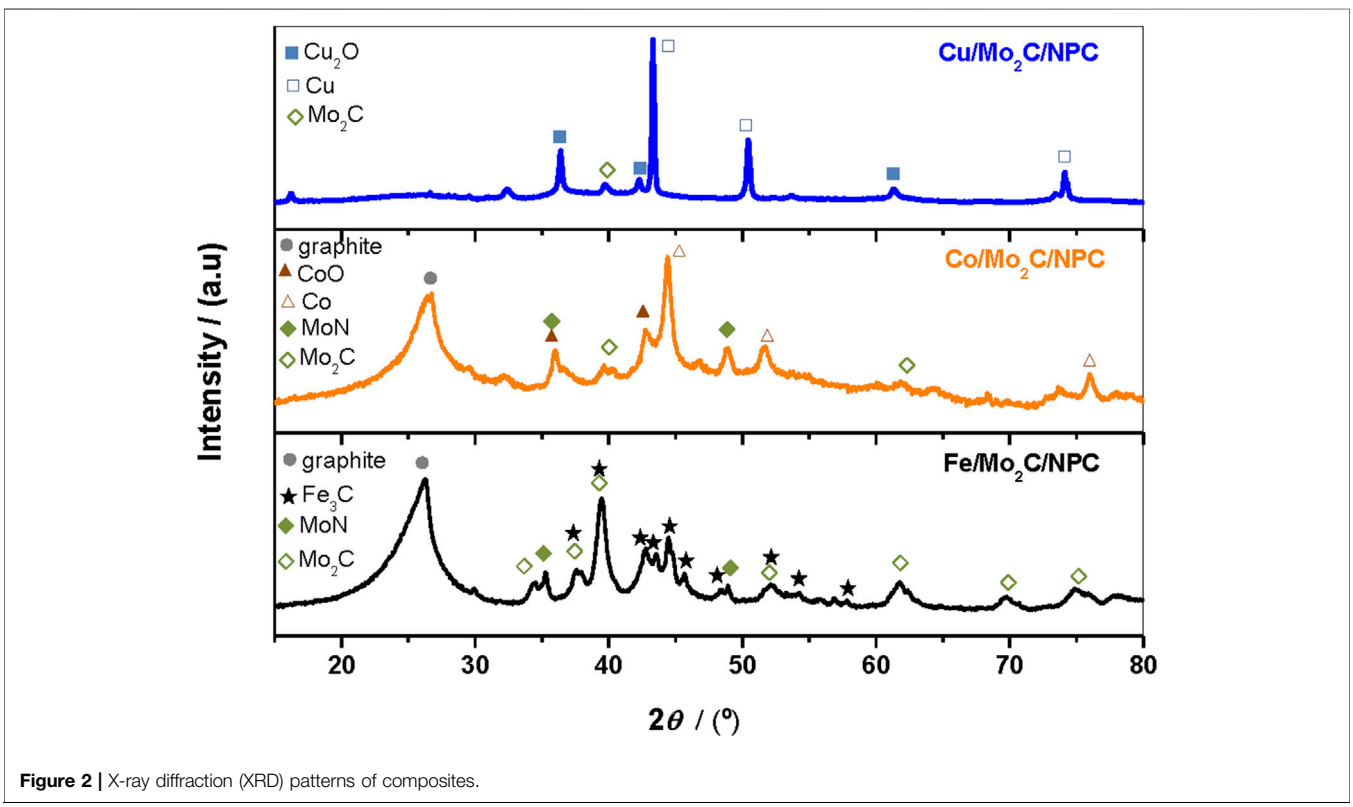

Figure 2 | X-ray diffraction (XRD) patterns of composites.

TABLE 1 | Surface elemental contents examined by XPS (wt.%)

Catalyst	C 1s	N 1s	Fe 2p	Co 2p	Cu 2p	P 2p	Mo 3d
Fe/Mo_2C/NPC	65	2.7	8.8	—	—	0.6	3.6
Co/Mo_2C/NPC	70	6.7	—	5.0	—	0.3	6.7
Cu/Mo_2C/NPC	47	5.0	—	—	25	0.9	7.9

Microscope spectrometer equipped with a laser beam emitting at 532 nm and 5 mW output power.

The electrochemical characterization of the composites was performed in a three-electrode cell system at room temperature controlled by an Autolab PGSTAT302N potentiostat-galvanostat. A glassy carbon rod and a reversible hydrogen electrode (RHE) were used as the counter electrode and the reference electrode, respectively. For the working electrode, a rotating ring-disk electrode (RRDE, PINE) with a glassy carbon disk with 0.196 cm^2 of area and a Pt ring was employed. The supporting electrolyte was 0.1M NaOH aqueous solution. The working electrode was prepared by adding 30 μL of catalytic ink. For the catalytic ink, 4 mg of composite was dispersed in 385 μL of Isopropyl alcohol (IPA) and water, IPA:H2O (1;1) solution and 15 μL of Nafion® (5 wt.%, Sigma-Aldrich) as a binder. For all measurements, N_2 (99.99%, Air Liquid) was employed to make an inert environment, and O_2 (99.99%, Air Liquid) was used for ORR measurements. In order to analyze the H_2O_2 yield, the ORR activity was performed while keeping the Pt ring at 1.2 V.

RESULTS AND DISCUSSION

X-ray diffractograms of electrocatalysts are shown in **Figure 2**. All composites show diffraction peaks corresponding to Mo_2C (JPCDS 00-035-0787), while MoN (JPCDS 01-077-1999) is observed in Co and Fe composites. The diffraction peak at 26.6° confirms the correct graphitization of carbon in the Fe and Co composites. However, the highest crystallinity of Cu_2O (JPCDS 01-077-0199) and Cu (JPCDS 00-001-1242) contrasts with the low crystallinity of the carbon in the Cu/Mo_2C/NPC composite. It seems that copper promotes a lower graphitization degree of the carbon during the pyrolysis process. Co/Mo_2C/NPC shows diffraction peaks assigned to Co (JPCDS 00-001-1255) and CoO (JPCDS 01-072-1474). A diffraction pattern of Fe_3C (JPCDS 00-034-0001) was also observed in the Fe/Mo_2C/NPC composite.

During the pyrolysis process, chitosan and melamine gradually decompose to several carbon-nitrogen intermediates. Functionalization chitosan biopolymer with melamine becomes effective due to the strong interaction between the pyranose units and the amine groups, which results in the crosslinked networks (Rybarczyk et al., 2015). It is also reported that the pyrolysis of melamine generates a series of intermediate condensed phases, such as so-called melem ($C_6N_7(NH_2)_3$) or graphitic carbon nitride materials (g-C_3N_4), and then further releases some chemically reactive hydrogen-, carbon-, and nitrogen-containing atomic species, such as $C_3N_3^+$,$C_2N_2^+$ and CN_2H^+, at higher temperatures (Huang et al., 2015). These reactive intermediates can behave as powerful reducing agents to reduce different metal oxides to metal carbide, nitride, or metallic particles during the pyrolysis treatment. Furthermore, the simultaneous formation of C=C species from intermediates is considered as the carbon source of graphite (Li et al., 2014b; Yang et al., 2015).

The surface elemental compositions and electronic configurations of the atoms in the composites were investigated by employing XPS. **Table 1** summarizes the chemical surface composition in weight % of the catalysts. It is important to note that the copper content on the surface far exceeds the Fe and Co surface content of the other two composites and is also more than twice the nominal value, which would indicate a poor dispersion or higher segregation of copper on the carbon matrix. The transition metal used (Fe, Co, or Cu) affects the amount of N, P, and Mo incorporated into the composite. Cobalt composite shows the higher surface N content (6,7 wt.%), and copper composite the higher amount of P (0.9 wt.%) and Mo (7.9 wt.%). All samples display low P content, being lower than 1 wt.%.

The high-resolution N1s and P2p XPS spectra of the composites were shown in **Figures 3A** and **B**, respectively. The N1s peak deconvolution of the three catalysts proposes three nitrogen components with the binding energies centered at about 398, 400, and 401 eV, corresponding to pyridinic N, pyrrolic N, and quaternary N, respectively. Additionally, in **Figure 3A**, the peak at the lower binding energy at 397 eV is assigned to Mo3p in all catalysts (Li et al., 2016). However, this peak could also be assigned to nitride species, such as MoN in cobalt and iron composites, according to XRD analysis. The P2p XPS spectra display a broad and low intensity peak centered at 133-133.5 eV, assigned to P-C (Razmjooei et al., 2014; Razmjooei et al., 2015). These XPS results indicate that N and P are incorporated into the carbon matrix in the three catalysts.

The spectra for Fe 2p, Co2p, and Cu2p core level are shown in **Figure 4**. The Fe2p spectra in **Figure 4A** shows peaks at 711.1 and 724.9 eV, which are assigned to Fe2p3/2 and Fe2p1/2 respectively Fe_3O_4 (Wagner et al., 1979). The surface oxidation of the iron samples does not allow the analysis of the inner layer, and therefore the detection of the iron carbide observed by XRD. Co2p shows binding energies of Co2p3/2 and Co2p1/2 at 782.3 and 798.1 eV, respectively, and the respective "satellite" peaks, which can be attributed to Co^{2+}–like species (Wagner et al., 1979; Luque-Centeno et al., 2020). The Cu2p core level spectra is displayed in **Figure 4C**. The main Cu2p3/2 signal is composed of two contributions at 932.7 and a shoulder at 934.4 eV, where the former is assigned to surface Cu^0 and the latter to Cu^{2+} with the respective satellite peaks (Wagner et al., 1979; Ania et al., 2015). In a similar way, the Mo3d core level spectra shows the thin oxidized layer on the molybdenum carbide surface and MoO_3 is only detected by XPS (not shown).

The TEM images of the NPC samples are displayed in **Figure 5**. All composites show metal particles embedded in an amorphous graphite structure. In Fe/Mo_2C/NPC, the nanoparticles are uniformly dispersed in the carbon matrix. This dispersion decreases in Co/Mo_2C/NPC and gets much worse in Cu/Mo_2C/NPC. Iron and cobalt composites show the presence of particles with average particle sizes between 10 and

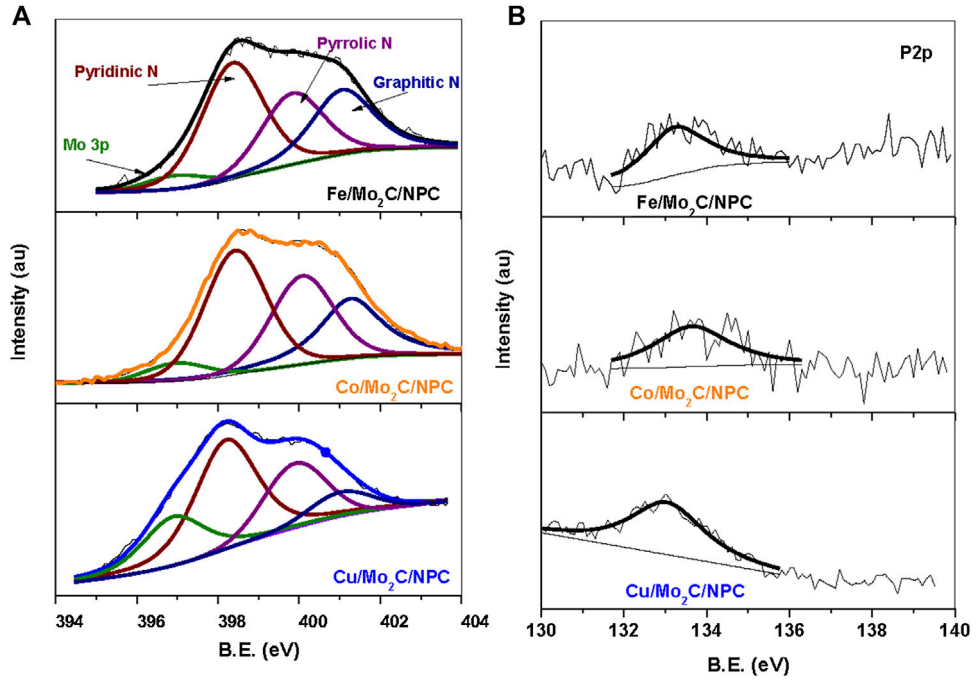

Figure 3 | High-resolution N1s XPS spectra **(A)** and P2p **(B)** of composites.

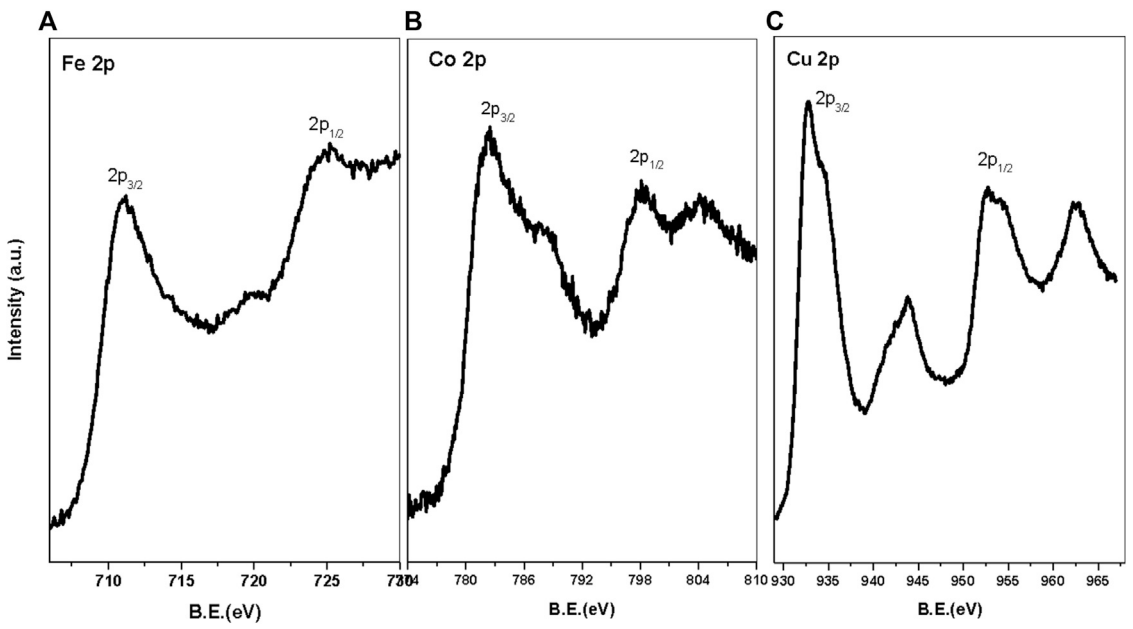

Figure 4 | High-resolution Fe 2p (**A**), Co 2p (**B**), and Cu 2p (**C**) XPS spectra.

30 nm cover of a thickness of the external carbon sheet. However, Cu/Mo_2C/NPC shows the presence of copper aggregates in the carbon matrix with an irregular morphology, and some metal nanoparticles outside of the carbon matrix (**Figure 5C**).

The Raman spectra of the composites show the characteristic peak corresponding to the D and G bands at 1350 cm^{-1} and 1580 cm^{-1}, respectively (**Figure 6**). The D band is assigned to the A1g breathing mode of disordered graphite structure and is due to the defect sites in

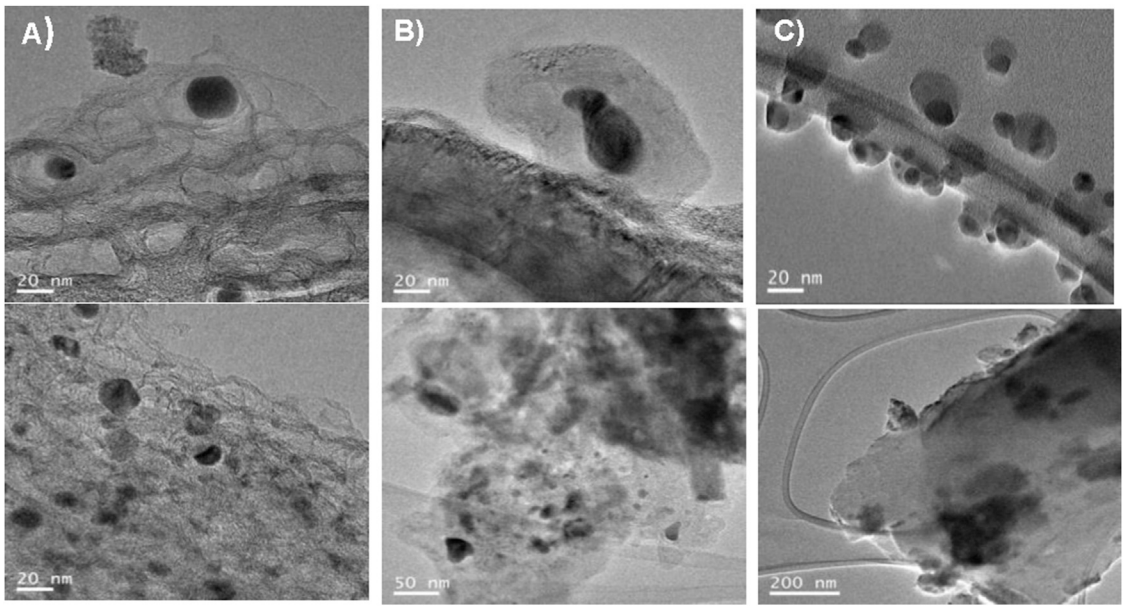

Figure 5 | TEM images of Fe/Mo2C/NPC **(A)**, Co/Mo2C/NPC **(B)**, and Cu/Mo2C/NPC **(C)**.

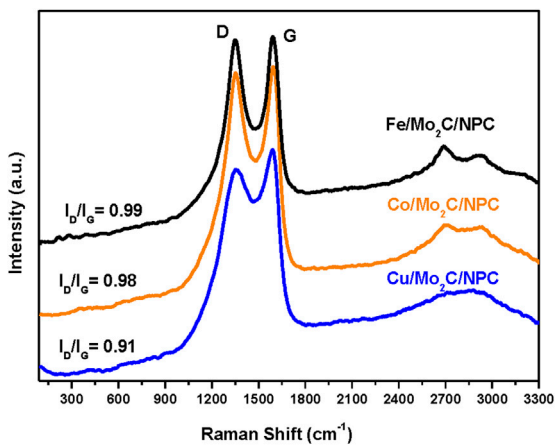

Figure 6 | Raman spectra of the composites. The calculated I_D/I_G values are also presented.

the hexagonal framework of graphite materials. The G band corresponds to the E2g stretching mode of graphite structure and denotes the sp^2 hybridized carbon atom structure (Yang et al., 2018). Both Raman bands have their corresponding overtones between 2500 and 3000 cm^{-1}, respectively. The height of the D peak usually increases upon chemical alteration of carbon structure. The ratio of D and G bands (I_D/I_G) is a good indicator of the disorder degree, graphitization, and crystallinity of the composites (values are indicated in **Figure 6**). It is observed that the I_D/I_G ratio is lower for the Cu (0.91) composite with respect to Co and Fe composites (ca. 0.99), which indicate a higher disorder degree and defects of the graphite formed in the latter catalysts. Certainly, several studies have established the relevance of defects, which seem to be one of the most challenging targets, in ORR electrocatalysis (Quílez-Bermejo et al., 2020). It is also observed that the intensity of the two-dimensional (2D) peak (~2690 cm^{-1}) increase in the Co composite and, particularly, in the Fe composite, revealing better graphitization of the carbon framework (Cheng et al., 2017). This suggests that the doping and graphitic structure of carbon matrix is not too dependent on the Co and Fe metal transition, but it changes with the copper metal.

The electrocatalytic activity of the composites was studied in alkaline media using a rotating ring-disk electrode (RRDE) technique with a rotation rate of 1,600 rpm. The key values for evaluating the ORR catalytic activity are the onset potential (obtained at -0.1 mA cm^{-2}), half-wave potential ($E_{1/2}$) and the diffusion-limiting current. The ORR activity and H_2O_2 yields of the electrocatalysts are displayed in **Figures 7A** and **B**, respectively. NPC was added for comparison. As evidenced in **Figure 7A** and **Table 2**, Fe/Mo_2C/NPC exhibits the best performance with an onset potential of 0.922 V (vs RHE) at -0.1 mA cm^{-2}, and limiting current density of -4.39 mA cm^{-2} at 0.2 V. In all other composites, the onset potential and limiting current gradually decreases from Co/Mo_2C/NPC (0.850 V, -3.57 mA cm^{-2}), NPC (0.714 V, -1.86 mA cm^{-2}), to Cu/Mo_2C/NPC (0.683 V, -1.64 mA cm^{-2}). It is observed that the plateau is inclined in all composites, which could indicate some diffusion limitations or inhomogeneous distribution of active sites on the electrode. The $E_{1/2}$ values can embody the capacity that a fuel cell cathode needs, holding a high working potential to provide high energy conversion efficiency. From **Table 2**, it can be seen that the Fe composite shows the highest $E_{1/2}$ value (0.811 V), further indicating the highly active nature of the Fe/Mo_2C/NPC towards ORR. These results demonstrate that the transition metal considerably affects the ORR activity in the Mo_2C/NPC

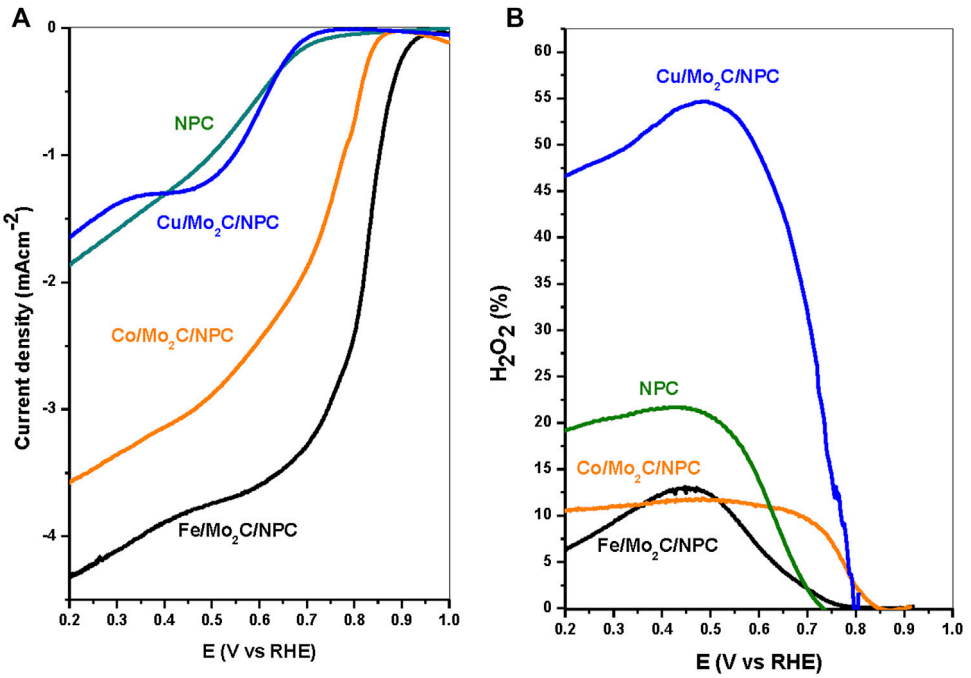

Figure 7 | ORR **(A)** and H2O2 yield **(B)** polarization curves for all catalysts at 1,600 rpm in 0.1 M NaOH, 10 mV s-1. The applied potential at the ring electrode was 1.2 V for the ORR.

TABLE 2 | Electrochemical parameters for ORR of the composites

Catalyst	E_{onset} (V) at -0.1 mA cm^{-2}	$E_{1/2}$(V)	J_L(mA cm^{-1}) at 0.2 V
Fe/Mo_2C/NPC	0.922	0.811	4.39
Co/Mo_2C/NPC	0.850	0.710	3.57
Cu/Mo_2C/NPC	0.683	0.576	1.64
NPC	0.714	0.502	1.86

composites. The polarization curves indicate that the Fe/Mo_2C/NPC catalyst has very high ORR activities and is comparable with conventional Pt/C catalysts, in which the onset potential is usually identified ca. 0.990 V (Jiang et al., 2015). Therefore, the gap between the onset potential of Fe/Mo_2C/NPC and the standard Pt/C is only 32 mV.

Based on the ring current generated from the oxidation of H_2O_2, we can observe that the Cu/Mo_2C/NPC catalyst produces a higher level of H_2O_2 (ca. 50%) than iron and cobalt composites do. The peroxide formations of the latter two are lower than 13% in all potential ranges studied. These results reveal that the Cu composite follows a combined 2-3 e^- electron-transfer number. In addition, the RRDE measurements reveal that the production of the corrosive H_2O_2 is highly suppressed on Fe/Mo_2C/NPC and Co/Mo_2C/NPC, promoting a $4e^-$ pathway. It is also observed that NPC produced a higher level of H_2O_2 compared to Fe- and Co-based composites. This may be due to how in free-metals-doped carbons, the carbon atoms next to heteroatoms exhibit excellent bonding ability to adsorb OOH, thus assisting the easy formation of the peroxide intermediate (Brouzgou et al., 2016; Sun et al., 2018).

Therefore, Fe/Mo_2C/NPC exhibits a higher onset potential and limiting current density, and has a selectivity of about four electrons in alkaline media, while Cu/Mo_2C/NPC has the lowest electron transfer number and worst ORR performance. These results indicate that Fe/Mo_2C/NPC composite is a promising electrocatalyst for H_2O production.

It is known that nitrogen and phosphorous dual-doped carbons improve the catalytic activity for ORR due to the synergetic effects (Choi et al., 2012; Li et al., 2015; Qiao et al., 2015). DFT simulations have demonstrated that quaternary nitrogen, along with phosphorus groups, are responsible for the improvement in the electrocatalytic activity in alkaline solution (Li et al., 2017). Also, the higher disorder degree and defects promoted by doped-carbons have revealed its significance in ORR activity (Quílez-Bermejo et al., 2020). According to our results, N and P are incorporated into the carbon matrix in the three composites. However, it has been shown that the transition metal is essential to obtain optimal carbon framework for ORR, with the copper being the one that promotes the formation of a less graphitized and defective carbon matrix during the synthetic process.

Furthermore, previous studies by our group show that the presence of the heteropolyacid HPMo can improve the ORR activity of graphene/chitosan composites compared to HPMo-free catalysts (Aghabarari et al., 2017). However, it should be pointed out that the order of surface N, P, and Mo amounts are not consistent with the catalyst's ORR performance. The Cu-composite has the highest Mo and P amounts and the second highest N amount, but it

has the lowest ORR performance. Clearly, the results obtained provide evidence of the important role played by each transition metal in the formation of active sites for ORR.

The Fe_3C encapsulated in dual-doped carbon materials seems to be an important active site (Yang et al., 2015; Ren et al., 2016). The outer protective graphitic layers stabilize the carbide nanoparticles, while the Fe_3C/Mo_2C nanoparticles should play a synergetic role in activating the outer surface of the graphitic layers towards the ORR. Such an enhanced catalytic activity has been explained from the large amounts of oxygen vacancies created by Mo_2C and Fe_3C as electron donors. On the other site, the outstanding ORR performance of Fe_3C-based ORR catalysts can be also attributable to the factors of the N dopants and Fe–N_x coordination species (Jiang et al., 2015). Furthermore, in this complex system we cannot rule out the presence of electrochemically active Fe-P interactions either. Recently, Razmjooei et al. found that the introduction of Fe on P-functionalized graphene caused remarkable synergistic effects, which were beneficial for ORR (Razmjooei et al., 2015). Therefore, these results highlighted the advantage of the facile synthetic approach to obtain a complex formed by Fe_3C along Mo_2C embedded in N- and P-dual doped carbon, which leads to significant ORR activity. However, the active sites of the Fe-related species need to be further elaborated, which is under progress.

CONCLUSIONS

In summary, a facile and cost-effective strategy for the production of Me/Mo_2C (Me = Fe, Co, Cu)-based composites embedded in N- and P-dual doped carbon matrices has been developed. For this end, inexpensive industrial materials, such as melamine and chitosan, as C and N sources and the heteropolyacid $H_3PMo_{12}O_{40}$ as P and Mo precursor were successfully used. Among transition metals considered, Fe gives rise to the best performing composite in carrying out the oxygen reduction reaction. It has been proposed that this enhanced ORR activity is due to the different synergistic effects obtained in the Fe_3C/Mo_2C species coordinated with N- and P-dual doped carbon. Therefore, this work is expected to improve the production of non-noble carbide-based heterostructure composites for practical applications in fuel cells and other applications, such as metal-air batteries.

DATA AVAILABILITY STATEMENT

The raw data supporting the conclusions of this article will be made available by the authors, without undue reservation.

AUTHOR CONTRIBUTIONS

B.A. conceptualization, methodology, investigation, materials. M.-C.S. analysis, interpretation. M.L. review, funding acquisition, suggestions. M.M.-H. supervision, logical interpretation, writing—review and editing.

ACKNOWLEDGMENTS

The authors acknowledge the Ministerio de Ciencia, Innovación y Universidades (MCIU), and FEDER for the funding received for the project, with references ENE2017-83976-C2-1-R, Spanish National Research Council COOPB20202, and MERC project 721399002.

REFERENCES

Aghabarari, B., Luque-Centeno, J. M., Capel-Sánchez, M., Lázaro Elorri, M. J., and Martínez-Huerta, M. V. (2019). Ni-based composites from chitosan biopolymer a one-step synthesis for oxygen evolution reaction. *Catalysts* 9, 471–481. doi:10.3390/catal9050471

Aghabarari, B., Martínez-Huerta, M. V., Ghiaci, M., Fierro, J. L. G., and Peña, M. A. (2013). Hybrid chitosan derviative-carbon support for oxygen reduction reactions. *RSC Adv.* 3, 5378–5381. doi:10.1016/j.ijhydene.2017.06.159

Aghabarari, B., Nezafati, N., Roca-Ayats, M., Capel-Sánchez, M. C., Lázaro, M. J., and Martínez-Huerta, M. V. (2017). Effect of molybdophosphoric acid in iron and cobalt graphene/chitosan composites for oxygen reduction reaction. *Int. J. Hydrogen Energy* 42, 28093-28101. doi:10.1016/j.ijhydene.2017.06.159

Ania, C. O., Seredych, M., Rodriguez-Castellon, E., and Bandosz, T. J. (2015). New copper/GO based material as an efficient oxygen reduction catalyst in an alkaline medium: the role of unique Cu/rGO architecture. *Appl. Catal. B Environ.* 163, 424–435. doi:10.1016/j.apcatb.2014.08.022

Brouzgou, A., Song, S., Liang, Z.-X., and Tsiakaras, P. (2016). Non-precious electrocatalysts for oxygen reduction reaction in alkaline media: latest achievements on novel carbon materials. *Catalysts* 6, 159.

Cheng, Y. H., Zhou, S. B., Hu, P., Zhao, G. D., Li, Y. X., Zhang, X. H., et al. (2017). Enhanced mechanical, thermal, and electric properties of graphene aerogels via supercritical ethanol drying and high-temperature thermal reduction. *Sci. Rep.* 7, 11. doi:10.1038/s41598-017-01601-x

Choi, C. H., Park, S. H., and Woo, S. I. (2012). Phosphorus-nitrogen dual doped carbon as an effective catalyst for oxygen reduction reaction in acidic media: effects of the amount of P-doping on the physical and electrochemical properties of carbon. *J. Mater. Chem.* 22, 12107–12115.

Chung, H. T., Won, J. H., and Zelenay, P. (2013). Active and stable carbon nanotube/nanoparticle composite electrocatalyst for oxygen reduction. *Nat. Commun.* 4, 1922. doi:10.1038/ncomms2944

Das, E., and Yurtcan, A. B. (2016). Effect of carbon ratio in the polypyrrole/carbon composite catalyst support on PEM fuel cell performance. *Int. J. Hydrogen Energy* 41, 13171–13179. doi:10.1016/j.ijhydene.2016.05.167

Fan, X., Liu, Y., Peng, Z., Zhang, Z., Zhou, H., Zhang, X., et al. (2017). Atomic H-induced Mo2C hybrid as an active and stable bifunctional electrocatalyst. *ACS Nano* 11, 384–394. doi:10.1021/acsnano.6b06089

Guil-López, R., Martínez-Huerta, M. V., Guillén-Villafuerte, O., Peña, M. A., Fierro, J. L. G., and Pastor, E. (2010). Highly dispersed molybdenum carbide as non-noble electrocatalyst for PEM fuel cells: performance for CO electrooxidation. *Int. J. Hydrogen Energy* 35. doi:10.1016/j.ijhydene.2010.05.044

Huang, K., Bi, K., Liang, C., Lin, S., Wang, W. J., Yang, T. Z., et al. (2015). Graphite carbon-supported Mo2C nanocomposites by a single-step solid state reaction for electrochemical oxygen reduction. *PLoS One* 10. doi:10.1371/journal.pone.0138330

Jaouen, F., Proietti, E., Lefevre, M., Chenitz, R., Dodelet, J.-P., Wu, G., et al. (2011). Recent advances in non-precious metal catalysis for oxygen-reduction reaction in polymer electrolyte fuel cells. *Energy Environ. Sci.* 4, 114–130. doi:10.1039/C0EE00011F

Jiang, H., Yao, Y., Zhu, Y., Liu, Y., Su, Y., Yang, X., et al. (2015). Iron carbide nanoparticles encapsulated in mesoporous Fe-N-doped graphene-like carbon

hybrids as efficient bifunctional oxygen electrocatalysts. *ACS Appl. Mater. Interfaces* 7, 21511–21520. doi:10.1021/acsami.5b06708

Khan, A., Goepel, M., Colmenares, J. C., and Gläser, R. (2020). Chitosan-based N-doped carbon materials for electrocatalytic and photocatalytic applications. *ACS Sustain. Chem. Eng.* 8, 4708–4727. doi:10.1021/acssuschemeng.9b07522

Li, J.-S., Wang, Y., Liu, C.-H., Li, S.-L., Wang, Y.-G., Dong, L.-Z., et al. (2016). Coupled molybdenum carbide and reduced graphene oxide electrocatalysts for efficient hydrogen evolution. *Nat. Commun.* 7, 11204. doi:10.1038/ncomms11204

Li, P., Qiu, Y., Liu, S., Li, H., Zhao, S., Diao, J., et al. (2019). Heterogeneous Mo 2 C/Fe 5 C 2 nanoparticles embedded in nitrogen-doped carbon as efficient electrocatalysts for the oxygen reduction reaction. *Eur. J. Inorg. Chem.* 2019, 3235–3241. doi:10.1002/ejic.201900390

Li, Q., Cao, R., Cho, J., and Wu, G. (2014a). Nanocarbon electrocatalysts for oxygen reduction in alkaline media for advanced energy conversion and storage. *Adv. Energy Mater.* 4, 1301415. doi:10.1002/aenm.201301415

Li, R., Cao, A., Zhang, Y., Li, G., Jiang, F., Li, S., et al. (2014b). Formation of nitrogen-doped mesoporous graphitic carbon with the help of melamine. *ACS Appl. Mater. Interfaces* 6, 20574–20578. doi:10.1021/am5061323

Li, R., Wei, Z., and Gou, X. (2015). Nitrogen and phosphorus dual-doped graphene/carbon nanosheets as bifunctional electrocatalysts for oxygen reduction and evolution. *ACS Catal.* 5, 4133–4142. doi:10.1021/acscatal.5b00601

Li, Z., Zhao, W., Yin, C., Wei, L., Wu, W., Hu, Z., et al. (2017). Synergistic effects between doped nitrogen and phosphorus in metal-free cathode for zinc-air battery from covalent organic frameworks coated CNT. *ACS Appl. Mater. Interfaces* 9, 44519–44528. doi:10.1021/acsami.7b14815

Liao, L., Bian, X., Xiao, J., Liu, B., Scanlon, M. D., and Girault, H. H. (2014). Nanoporous molybdenum carbide wires as an active electrocatalyst towards the oxygen reduction reaction. *Phys. Chem. Chem. Phys.* 16, 10088–10094. doi:10.1039/c3cp54754j

Liu, Z., Zhang, G., Lu, Z., Jin, X., Chang, Z., and Sun, X. (2013). One-step scalable preparation of N-doped nanoporous carbon as a high-performance electrocatalyst for the oxygen reduction reaction. *Nano Res.* 6, 293–301. doi:10.1007/s12274-013-0307-9

Luque-Centeno, J. M., Martínez-Huerta, M. V., Sebastián, D., Pardo, J. I., and Lázaro, M. J. (2020). CoTiO3/NrGO nanocomposites for oxygen evolution and oxygen reduction reactions: synthesis and electrocatalytic performance. *Electrochim. Acta* 331, 135396–135407. doi:10.1016/j.electacta.2019.135396

Marguerite, R. (2006). Chitin and chitosan: properties and applications. *Prog. Polym. Sci.* 31, 603–632.

Martínez-Huerta, M. V., and Lázaro, M. J. (2017). Electrocatalysts for low temperature fuel cells. *Catal. Today* 285, 3–12. doi:10.1016/j.cattod.2017.02.015

Palaniselvam, T., Kashyap, V., Bhange, S. N., Baek, J.-B., and Kurungot, S. (2016). Nanoporous graphene enriched with Fe/Co-N active sites as a promising oxygen reduction electrocatalyst for anion exchange membrane fuel cells. *Adv. Funct. Mater.* 26, 2150–2162. doi:10.1002/adfm.201504765

Pan, T., Liu, H., Ren, G., Li, Y., Lu, X., and Zhu, Y. (2016). Metal-free porous nitrogen-doped carbon nanotubes for enhanced oxygen reduction and evolution reactions. *Sci. Bull.* 61, 889–896. doi:10.1007/s11434-016-1073-3

Peng, H., Liu, F., Liu, X., Liao, S., You, C., Tian, X., et al. (2014). Effect of transition metals on the structure and performance of the doped carbon catalysts derived from polyaniline and melamine for ORR application. *ACS Catal.* 4, 3797–3805. doi:10.1021/cs500744x

Qiao, M., Tang, C., He, G., Qiu, K., Binions, R., Parkin, I. P., et al. (2016). Graphene/nitrogen-doped porous carbon sandwiches for the metal-free oxygen reduction reaction: conductivity versus active sites. *J. Mater. Chem. A* 4, 12658–12666. doi:10.1039/c6ta04578b

Qiao, X., Liao, S., You, C., and Chen, R. (2015). Phosphorus and nitrogen dual doped and simultaneously reduced graphene oxide with high surface area as efficient metal-free electrocatalyst for oxygen reduction. *Catalysts* 5, 981–991. doi:10.3390/catal5020981

Quílez-Bermejo, J., Morallón, E., and Cazorla-Amorós, D. (2020). Metal-free heteroatom-doped carbon-based catalysts for ORR. A critical assessment about the role of heteroatoms. *Carbon N. Y.* 165, 434–454. doi:10.1016/j.carbon.2020.04.068

Razmjooei, F., Singh, K. P., Bae, E. J., and Yu, J. S. (2015). A new class of electroactive Fe- and P-functionalized graphene for oxygen reduction. *J. Mater. Chem. A* 3, 11031–11039. doi:10.1039/c5ta00970g

Razmjooei, F., Singh, K. P., Song, M. Y., and Yu, J.-S. (2014). Enhanced electrocatalytic activity due to additional phosphorous doping in nitrogen and sulfur-doped graphene: a comprehensive study. *Carbon N. Y.* 78, 257–267. doi:10.1016/j.carbon.2014.07.002

Ren, G., Lu, X., Li, Y., Zhu, Y., Dai, L., and Jiang, L. (2016). Porous core-shell Fe3C embedded N-doped carbon nanofibers as an effective electrocatalysts for oxygen reduction reaction. *ACS Appl. Mater. Interfaces* 8, 4118–4125. doi:10.1021/acsami.5b11786

Roca-Ayats, M., García, G., Peña, M. A., and Martínez-Huerta, M. V. (2014). Titanium carbide and carbonitride electrocatalyst supports: modifying Pt-Ti interface properties by electrochemical potential cycling. *J. Mater. Chem. A* 2. doi:10.1039/c4ta03782k

Rybarczyk, M. K., Lieder, M., and Jablonska, M. (2015). N-doped mesoporous carbon nanosheets obtained by pyrolysis of a chitosan-melamine mixture for the oxygen reduction reaction in alkaline media. *RSC Adv.* 5, 44969–44977. doi:10.1039/c5ra05725f

Shao, M., Chang, Q., Dodelet, J.-P., and Chenitz, R. (2016). Recent advances in electrocatalysts for oxygen reduction reaction. *Chem. Rev.* 116, 3594–3657. doi:10.1021/acs.chemrev.5b00462

Sheng, Z.-H., Shao, L., Chen, J.-J., Bao, W.-J., Wang, F.-B., and Xia, X.-H. (2011). Catalyst-free synthesis of nitrogen-doped graphene via thermal annealing graphite oxide with melamine and its excellent electrocatalysis. *ACS Nano* 5, 4350–4358. doi:10.1021/nn103584t

Stephens, I. E. L., Bondarenko, A. S., Gr+©nbjerg, U., Rossmeisl, J., and Chorkendorff, I. (2012). Understanding the electrocatalysis of oxygen reduction on platinum and its alloys. *Energy Environ.Sci.* 5, 6744–6762. doi:10.1039/C2EE03590A

Sun, Y., Sinev, I., Ju, W., Bergmann, A., Dresp, S., Kühl, S., et al. (2018). Efficient electrochemical hydrogen peroxide production from molecular oxygen on nitrogen-doped mesoporous carbon catalysts. *ACS Catal.* 8, 2844–2856. doi:10.1021/acscatal.7b03464

Wagner, C. D., Riggs, W. M., Davis, L. E., and Moulder, J. F. (1979). *Handbook of X-ray photoelectron spectroscopy.* , ed. G. E. Muilenberg Minnesota: Perkin-Elmer Corporation.

Wang, X. X., Swihart, M. T., and Wu, G. (2019). Achievements, challenges and perspectives on cathode catalysts in proton exchange membrane fuel cells for transportation. *Nat. Catal.* 2, 578–589. doi:10.1038/s41929-019-0304-9

Wu, G., More, K. L., Johnston, C. M., and Zelenay, P. (2011). High-performance electrocatalysts for oxygen reduction derived from polyaniline, iron, and cobalt. *Science* 332, 443–447.

Wu, T. X., Wang, G. Z., Zhang, X., Chen, C., Zhanga, Y. X., and Zhao, H. J. (2015). Transforming chitosan into N-doped graphitic carbon electrocatalysts. *Chem. Commun.* 51, 1334–1337. doi:10.1039/c4cc09355k

Xie, S. L., Huang, S. C., Wei, W. J., Yang, X. Z., Liu, Y., Lu, X. H., et al. (2015). Chitosan waste-derived Co and N Co-doped carbon electrocatalyst for efficient oxygen reduction reaction. *ChemElectroChem* 2, 1806–1812. doi:10.1002/celc.201500199

Yang, W., Liu, X., Yue, X., Jia, J., and Guo, S. (2015). Bamboo-like carbon nanotube/Fe3C nanoparticle hybrids and their highly efficient catalysis for oxygen reduction. *J. Am. Chem. Soc.* 137, 1436–1439. doi:10.1021/ja5129132

Yang, X., Xu, Y., Xue, B., Jiang, Y., and Li, F. (2018). Cordierite reinforced graphite nanocomposite with superior adsorption capacity synthesized by in-situ carbon-bed pyrolysis method. *Microporous Mesoporous Mater.* 265, 219–226. doi:10.1016/j.micromeso.2018.02.019

Yasuda, S., Furuya, A., Uchibori, Y., Kim, J., and Murakoshi, K. (2016). Iron-nitrogen-doped vertically aligned carbon nanotube electrocatalyst for the oxygen reduction reaction. *Adv. Funct. Mater.* 26, 738–744. doi:10.1002/adfm.201503613

Zhang, Y., Li, C., Chen, Z., Ni, Y., Kong, F., Kong, A., et al. (2017). Ionic liquid-derived MoC nanocomposites with ordered mesoporosity as efficient Pt-free electrocatalyst for hydrogen evolution and oxygen reduction. *Catal. Letters* 147, 253–260. doi:10.1007/s10562-016-1914-3

Zhong, Y., Xia, X. H., Shi, F., Zhan, J. Y., Tu, J. P., and Fan, H. J. (2015). Transition metal carbides and nitrides in energy storage and conversion. *Adv. Sci.* 3, 1500286. doi:10.1002/advs.201500286

Conflict of Interest: The authors declare that the research was conducted in the absence of any commercial or financial relationships that could be construed as a potential conflict of interest.